Published in final edited form as:
Hum Brain Mapp. 2015 December ; 36(12): 5183–5195. doi:10.1002/hbm.23003.

Spatiotemporal Patterns of Cortical Fiber Density in Developing Infants, and Their Relationship with Cortical Thickness

Gang Li[1], **Tianming Liu**[2], **Dong Ni**[3], **Weili Lin**[1], **John H. Gilmore**[4], and **Dinggang Shen**[1,5,*]

[1]Department of Radiology and BRIC, University of North Carolina at Chapel Hill, NC, 27599, USA

[2]Department of Computer Science and Bioimaging Research Center, The University of Georgia, Athens, GA, 30602, USA

[3]The Guangdong Key Laboratory for Biomedical Measurements and Ultrasound Imaging, Department of Biomedical Engineering, Shenzhen University, Shenzhen 518060, China

[4]Department of Psychiatry, University of North Carolina at Chapel Hill, NC, 27599, USA

[5]Department of Brain and Cognitive Engineering, Korea University, Seoul, Republic of Korea

Abstract

The intrinsic relationship between the convoluted cortical folding and the underlying complex whiter matter fiber connections has received increasing attention in current neuroscience studies. Recently, the axonal pushing hypothesis of cortical folding has been proposed to explain the finding that the axonal fibers (derived from diffusion tensor images) connecting to gyri are significantly denser than those connecting to sulci in both adult human and non-human primate brains. However, it is still unclear about the spatiotemporal patterns of the fiber density on the cortical surface of the developing infant brains from birth to 2 years of age, which is the most dynamic phase of postnatal brain development. In this paper, for the first time, we systemically characterized the spatial distributions and longitudinal developmental trajectories of the cortical fiber density in the first 2 postnatal years, via joint analysis of longitudinal structural and diffusion tensor imaging from 33 healthy infants. We found that the cortical fiber density increases dramatically in the first year and then keeps relatively stable in the second year. Moreover, we revealed that the cortical fiber density on gyral regions was significantly higher at 0, 1, and 2 years of age than that on sulcal regions in the frontal, temporal and parietal lobes. Meanwhile, the cortical fiber density was strongly positively correlated with cortical thickness at several 3-hinge junction regions of gyri. These results significantly advanced our understanding of the intrinsic relationship between the cortical folding, cortical thickness and axonal wiring during early postnatal stages.

Keywords

Infant; cortical surface; fiber density; cortical folding; cortical thickness; longitudinal development

---

[*]Corresponding Author: Dinggang Shen, dgshen@med.unc.edu, 1-919-843-5420, Radiology and BRIC, UNC-Chapel Hill School of Medicine, Bioinformatics Building 3117, 130 Mason Farm Road, Chapel Hill, NC 27599.

The authors declare no conflict of interest.

1. Introduction

The human cerebral cortex is characterized by the highly convoluted cortical folding, composed of concave sulci and convex gyri (Carman, et al. 1995; Ono, et al. 1990; Van Essen and Drury 1997; Zilles, et al. 1989), and their underlying complicated axonal connections (Nie, et al. 2012a; Van Essen 1997). Recently, the intrinsic relationship between these two characteristic attributes has received increasing attention in neuroscience studies, though the answer remains largely unclear. During the third trimester of fetal life, the human cerebral cortex grows dramatically from a relatively smooth, lissencephalic structure into a convoluted structure, largely resembling the morphology of the adult brain (Armstrong, et al. 1995; Hill, et al. 2010). It has been hypothesized that the axonal wiring is a critical driving force forming the convoluted cortical folding (Van Essen 1997). In recent neuroimaging studies of both adult human and non-human primate brains, the terminations of axonal fibers derived from diffusion tensor imaging (DTI) data were found to dominantly concentrate on convex gyri, relative to the concave sulci (Chen, et al. 2013; Li, et al. 2010; Nie, et al. 2012a). This finding has also been replicated in a range of mammalian brains via DTI and high angular resolution diffusion imaging (HARDI) (Nie, et al. 2012a; Zhang, et al. 2014), including the recently released Human Connectome Project data (Zhang, et al. 2014). Moreover, structural fiber connection patterns were found to closely follow gyral folding patterns in the neocortices of macaque, chimpanzee, and human brains, despite the progressively increased complexity and variability of cortical folding and structural connection patterns during evolution (Chen, et al. 2013). In parallel, at the cellular and molecular levels, a recent joint study of the Allen Mouse Brain Connectivity Atlas and the Allen Mouse Brain Atlas demonstrated that the cerebellum gyri and sulci of rodent brains are significantly different in both axonal connectivity and gene expression patterns (Zeng, et al. 2014). However, all these findings cannot be well explained by the popular tension-based theory of morphogenesis, which posits that the cortical regions strongly interconnected by wiring axons are pulled towards one another to form a gyral fold (Van Essen 1997), thus implying that axonal fibers should concentrate on sulci rather than on gyri. To bridge this significant gap, the axonal pushing hypothesis of cortical folding has been proposed, which implies that gyri should have a higher density of fiber connection than sulci (Chen, et al. 2013; Nie, et al. 2012a).

However, all prior studies of the cortical fiber density that supported the axonal pushing hypothesis have focused on adult brains, with both cortical folding and axonal wiring being well developed (Chen, et al. 2013; Nie, et al. 2012a). Therefore, it is still unclear how the cortical fiber density *spatially* distributes and *longitudinally* develops on the cortical surface of developing infants from birth to 2 years of age, which is the most dynamic and critical phase of postnatal structural and functional development of the human cerebral cortex (Choe, et al. 2013; Gao, et al. 2009b; Gilmore, et al. 2012; Hazlett, et al. 2011; Holland, et al. 2014; Knickmeyer, et al. 2008; Li, et al. 2013; Lyall, et al. 2015; Meng, et al. 2014; Nie, et al. 2012b; Qiu, et al. 2015; Sadeghi, et al. 2013). At term birth, major cortical sulcal-gyral folding and long-range axonal connections are already present (Chi and Dooling 1976; Dubois, et al. 2008a; Hill, et al. 2010; Kostovic and Jovanov-Milosevic 2006; Takahashi, et al. 2012). In the first postnatal year, cortical surface area expands approximately 80% (Li, et al. 2013) and cortical thickness increase about 42% (Li, et al. 2015a), with regionally heterogeneous growth patterns, accompanied with dynamic white matter myelination and maturation (Geng, et al. 2012; Qiu, et al. 2015; Sadeghi, et al. 2013). Many neurodevelopmental and neuropsychiatric disorders are hypothesized to be the consequences of abnormal brain development during this critical period of dynamic cortex growth (Gilmore, et al. 2012; Grewen, et al. 2014; Hazlett, et al. 2011; Lyall, et al. 2015; Wolff, et al. 2015; Wolff, et al. 2012). Therefore, studying the cortical fiber density during this period would greatly advance our understanding of the intrinsic relationship between cortical folding and fiber connection during their dynamic development, and also provide important insights into the neurodevelopmental disorders with abnormal cortical folding or axonal connection. Motivated by these reasons, for the first time (as far as we know), this study aims to systematically investigate the spatial distributions and longitudinal development of the cortical fiber density by using 33 healthy infants, each with both longitudinal structural and diffusion tensor imaging scans at birth, 1 year, and 2 years of age. Moreover, the relationship between the cortical fiber density and cortical thickness, which is an important cortical anatomical attribute related to normal development, cognitive functioning, and neurodevelopmental and neuropsychiatric disorders (Fischl and Dale 2000; Li, et al. 2015a; Lyall, et al. 2015; Nie, et al. 2013; Rimol, et al. 2010; Shaw, et al. 2008; Shaw, et al. 2006; Sowell, et al. 2004), was also quantitatively characterized across the whole cortex at each of the three ages.

2. Materials and Methods

Subjects

This study was approved by the Institutional Review Board of the University of North Carolina (UNC)-Chapel Hill. Pregnant mothers were recruited during the second trimester of pregnancy from the UNC hospitals. Informed written consents were obtained from all parents. Exclusion criteria included abnormalities on fetal ultrasound, gestational age at birth < 32 weeks, major medical or neurologic illness after birth, and major medical or psychotic illness in the mother (Gilmore, et al. 2012; Yap, et al. 2011).

In total, 33 normal developing infants (16 males and 17 females) were included in this study, with each infant being longitudinally scanned three times at 0, 1, and 2 years of age. The gestational ages at MRI scans were: 41.4 ± 1.6 weeks, 94.5 ± 2.4 weeks and 144.7 ± 4.5 weeks for 0, 1, and 2 years of age, respectively. This infant dataset has been used in previous studies on longitudinal development of cortical structural networks (Nie, et al. 2014; Yap, et al. 2011).

MR Image Acquisition

Longitudinal T1, T2 and diffusion-weighted MR images were acquired using a Siemens 3T head-only scanner (Allegra, Siemens Medical System, Erlangen, Germany) with a circular polarized head coil. All infants were scanned unsedated while asleep, fitted with ear protection and with their heads secured in a vacuum-fixation device. T1-weighted images (160 sagittal slices) were acquired by using the imaging parameters: TR = 1900 ms, TE = 4.38 ms, inversion time = 1100 ms, flip angle = 7°, and resolution = $1 \times 1 \times 1$ mm^3. T2-

weighted images (70 transverse slices) were acquired using the parameters: TR = 7380 ms, TE = 119 ms, flip angle = 150°, and resolution = 1.25×1.25×1.95 mm^3. Diffusion-weighted images (45 axial slices) were acquired with the parameters: TR/TE = 5200/73 ms, acquisition matrix = 128 × 96, voxel resolution = 2 × 2 × 2 mm^3, one image without diffusion gradient (b = 0), and 6 non-collinear diffusion gradient directions at b-value = 1000 s/mm^2. To improve the signal-to-noise ratio, for each subject, a single DWI volume was obtained by combing five repeated sequences after motion correction.

Image Preprocessing

All images were visually inspected to ensure reasonable quality before analysis. All structural MR images were preprocessed using an infant-specific computational pipeline as detailed in (Li, et al. 2013; Li, et al. 2014b; Li, et al. 2014d). Briefly, it includes the following major steps: 1) skull stripping by a learning-based method (Shi, et al. 2012) and removal of cerebellum and brain stem by registration with an atlas (Shen and Davatzikos 2002); 2) correction of intensity inhomogeneity using N3 (Sled, et al. 1998); 3) rigid alignment onto the age-specific infant brain atlas (Shi, et al. 2011); 4) tissue segmentation of infant brain MR images using an infant-dedicated longitudinally-guided coupled level-set method (Wang, et al. 2013a; Wang, et al. 2013b); 5) masking and filling non-cortical structures, and separation of each brain into left and right hemispheres.

For DTI images, after distortion correction, diffusion tensors were first constructed by a weighted least squares estimation method (Basser, et al. 1994; Zhu, et al. 2007) and the fractional anisotropy (FA) map was then computed (Yap, et al. 2011). Next, a whole-brain streamline tractography was conducted on each DTI image in its native space with the following parameters: the minimal seed point FA of 0.2, minimal allowed FA of 0.1, maximal turning angle of 70°, minimal fiber length of 20 mm, and maximal fiber length of 200 mm (Yap, et al. 2011). The motivation of using a low FA threshold was to ensure that unmyelinated white matter fibers could be reasonably extracted in infant brains. To align structural images with DTI, for each subject, T2 image was rigidly aligned onto the b0 image. All alignment results were visually inspected to ensure the quality. This transformation matrix was also used to transform cortical surfaces reconstructed from structural images onto the DTI space in the following sections.

Cortical Surface Reconstruction and Registration

Cortical surface reconstruction and registration were performed by an infant-specific computational pipeline for cortical surface-based analysis, which has been extensively verified on more than 500 infant brain MR images (Li, et al. 2014a; Li, et al. 2013; Li, et al. 2015b; Li, et al. 2014c; Lyall, et al. 2015). Specifically, for each hemisphere of each image, cortical surfaces represented by triangular meshes were reconstructed by using a topology-preserving deformable surface method (Li, et al. 2014a; Li, et al. 2012), based on tissue segmentation results. Specifically, the inner cortical surface (white/gray matter interface) was first reconstructed by topology correction of the white matter and then tessellation of the corrected white matter as a triangular mesh. To address the severe partial volume effects in the tight sulci of small-sized infant brain MRI, which might result in incorrect reconstruction of the outer cortical surface, explicit thin separations between opposite tight sulci were further recovered (Li, et al. 2014a; Li, et al. 2012). Next, the inner cortical surface was deformed using forces derived from Laplace’s equation to reconstruct the outer cortical surface by preserving its initial topology and also avoiding surface mesh self-intersection (Li, et al. 2014a; Li, et al. 2012). The cortical thickness of each vertex was then computed as the average value of the minimum distance from inner to outer surfaces and the minimum distance from outer to inner surfaces. The inner cortical surface was also parcellated as four lobes, i.e., frontal, parietal, temporal, and occipital lobes, and then segmented as sulcal regions and gyral regions (Li, et al. 2009), respectively. For cortical surface registration, the inner cortical surface was further smoothed, inflated, and mapped to a sphere by minimizing the metric distortion between the cortical surface and its spherical representation (Fischl, et al. 1999).

To determine longitudinal vertex-to-vertex cortical correspondences, for each hemisphere of each subject, its spherical cortical surface at the i-th ($i \in 0, 1$) year of age was aligned onto its corresponding cortical surface at the i+1-th years of age by using Spherical Demons based on the cortical folding geometries (Yeo, et al. 2010). For each hemisphere of each subject, the deformation field from 0 to 2 years of age was then computed by concatenating the deformation map from 0 to 1 year of age and that from 1 to 2 years of age (Li, et al. 2013). To establish unbiased cross-sectional vertex-to-vertex cortical correspondences, for each hemisphere, group-wise registration of spherical cortical surfaces of all subjects at 2 years of age were performed by using Spherical Demons (Yeo, et al. 2010). For each hemisphere, the inner cortical surface of each subject at 2 years of age was resampled to a standard-mesh tessellation based on the deformation field obtained from the group-wise surface registration, thus establishing the vertex-to-vertex correspondences across all subjects at 2 years of age. Based on the longitudinal surface registration results of each subject, the standard-mesh tessellation of each subject at 2 years of age was further warped to 1 year of age and 0 year of age, respectively, thereby establishing the longitudinal vertex-to-vertex cortical correspondences. Hence, for each hemisphere, inner cortical surfaces of all subjects across all ages were represented by the same standard mesh tessellation, thus establishing both longitudinal and cross-sectional vertex-to-vertex cortical correspondences. All cortical surface reconstruction and registration results have been visually inspected to ensure reasonable quality.

Computing Fiber Density on Cortical Surfaces

Based on the streamline tractography results, fibers were connected onto the resampled inner cortical surfaces to measure the fiber density (Nie, et al. 2012a; Zhang, et al. 2010). Note that the extracted fibers could be *either* outside the inner cortical surface when the gray matter is over-segmented, *or* inside the inner cortical surface when the gray matter is under-segmented. To address this issue, if an end point of a fiber is outside of the inner cortical surface, the connection point of this fiber was located by searching along the fiber backwards the inner cortical surface. Otherwise, the connection point was searched by extending the fiber towards the inner cortical surface. The searching procedure stopped either when the connection point was found, or a searching threshold of 20mm was exceeded (Nie, et al. 2014). After the above procedure, any fibers that cannot reach the inner cortical surface were discarded. For each vertex on the inner cortical surface, the fiber density was then defined as the number of fibers connected to a unit area (mm^2). Figure 1 shows the computed cortical fiber density on a representative infant at 0, 1, and 2 years of age.

3. Results

Spatial distributions of cortical fiber density at 0, 1 and 2 years of age

Figure 2 shows the vertex-wise spatial distribution of the average fiber density on cortical surfaces from 33 infants at 0, 1, and 2 years of age. As shown in Figure 2, the cortical surface exhibits regionally heterogeneous patterns of fiber density at the three ages. In general, gyri have higher fiber density than sulci, which is particularly pronounced in the frontal lobe. Figure 3 provides the scatter plots of the average cortical fiber density on sulci and gyri separately across the whole cortex of the 33 subjects. As we can see from Figure 2 and Figure 3, the cortical fiber density increases dramatically in the first year and then increases relatively small in the second year. Specifically, in the first year, the cortical fiber density increases 112% on sulci and 99% on gyri. In contrast, in the second year, the cortical fiber density only increases 10% on sulci and 16% on gyri. To further investigate the region-specific patterns of the cortical fiber density between sulci and gyri, Figure 4 shows the mean and standard deviation of the cortical fiber density on each of the four lobes, i.e., frontal, parietal, temporal, and occipital lobes, and also on the whole cortex from the 33 infants at 0, 1, and 2 years of age. Among the four lobes, the frontal lobe consistently exhibits the highest fiber density on gyri, whereas the occipital lobe consistently shows the lowest fiber density on gyri from 0 to 2 years of age. Table 1 shows the ratios of the cortical fiber density on gyri *vs* that on sulci at 0, 1, and 2 years of age. The frontal and temporal cortices consistently exhibit high ratios of the cortical fiber density between gyri and sulci, whereas the occipital cortex consistently exhibits low ratios. Table 2 further provides the statistical significance of the cortical fiber density difference between gyri and sulci in the first two years of age, by using paired t-test. Specifically, in the frontal, temporal, and parietal lobes, the fiber density on gyri is statistically significantly higher than that on sulci ($p < 0.05$) consistently at 0, 1, and 2 years of age. In contrast, in the occipital lobe, there is no significant difference on the fiber density between sulci and gyri at 0 year of age. Moreover, the fiber density on gyri is even significantly lower than that on sulci on both hemispheres at 1 year of age, and also on the right hemisphere at 2 years of age ($p < 0.05$).

Relationship between fiber density and cortical thickness in infants

Cortical thickness is an important anatomical attribute of the cortex, and is related to normal development and aging, cognitive functioning, and neuropsychiatric disorders (Lyall, et al. 2015). For illustration, Figure 5 provides the scatter plots of the average cortical thickness on sulci and gyri separately across the whole cortex of the 33 subjects. As we can see, cortical thickness increases dramatically in the first year and then changes very subtly in the second year. However, the relationship between the cortical fiber density and cortical thickness has not been studied before. Herein, for the first time, the Pearson's correlation coefficient between these two distinct cortical attributes was computed for each vertex across the whole cortex for each age group, as shown in Figure 6. Note that, before the correlation analysis, a linear regression was performed at each vertex of each age to remove the effects of multiple confounding variables: age, gender and overall mean values (He, et al. 2007; Nie, et al. 2014). The residuals were then treated as the raw values for correlation analysis. As we can see from Figure 6, the correlation coefficients of the fiber density and cortical thickness were age-related and regionally heterogeneous across the cortex. Interestingly, many junction regions of gyri, e.g., the junction between percentral and middle temporal gyri, and the junction between percentral and superior temporal gyri, exhibited strong positive correlations between the cortical fiber density and cortical thickness in the first two years of age, as pointed out by red arrows in Figure 6.

4. Discussion

It has been shown that the cortical fiber density increased dramatically in the first year and then increased relatively small in the second year. At term birth, although long-range axonal connection are already present (Kostovic and Jovanov-Milosevic 2006; Takahashi, et al. 2012), the white matter has a low degree of myelination (Dubois, et al. 2008b; Dubois, et al. 2006; Geng, et al. 2012), thus leading to a small number of fibers approaching the cortex using the streamline fiber tracking. Then, the white matter undergoes dynamic myelination and maturation in the first year, relative to the second year, resulting in much more tracked fibers connecting to the cortex at 1 year and 2 years of age, compared to 0 year of age. The more dynamic increase of the cortical fiber density in the first year relative to the second year is also consistent with the finding that the cortical folding degree grows more rapidly in the first year than the second year (Li, et al. 2014d), indicating the existence of intrinsic relationship between the cortical folding and axonal connectivity. In addition, our result is consistent with the finding that the change of diffusion indices derived from DTI is much more dynamic in the first year than in the second year (Gao, et al. 2009a; Geng, et al. 2012).

Our results have shown that the cortical fiber density on gyri was significantly higher at 0, 1, and 2 years of age than that on sulci in the frontal, temporal, and parietal lobes, which is consistent with the findings in adult brains and also strongly supports the recent axonal pushing hypothesis of cortical folding (Nie, et al. 2012a). However, in contrast to other lobes, the cortical fiber density on gyri in the occipital lobe (visual cortex) was not significantly different from that on sulci at 0 year of age. Moreover, the fiber density on gyri was significantly lower than that on sulci at 1 year and 2 years of age. This may suggest regionally varying relationship between the cortical folding and axonal wiring, which, however, needs to be further verified in the adult human and non-human primate brains. This result might also suggest that there could be multiple cortical folding mechanisms interacting with each other in different brain areas and during different stages of neurodevelopment (Van Essen 2013; Zilles, et al. 2013). Notably, the “gyral bias” concept (Van Essen 2014) cannot explain the inverted gyral/sulcal fiber density patterns in the occipital lobe here. And recent studies have suggested that the macro-scale DTI-derived fiber connection patterns largely agree with the meso-scale axonal connection patterns mapped via anterograde tracers coupled with serial two-photon tomography (Chen, et al. 2015).

Similar to the developmental pattern of the cortical fiber density, cortical thickness also increased dynamically in the first year and relatively subtle in the second year (Li, et al.

2015a), reflecting the underlying age-specific cytoarchitectural changes of the cortex. Also, cortical thickness on gyri is generally larger than that on sulci in adults (Fischl and Dale 2000), resembling the spatial distribution of cortical fiber density and also reflecting distinct cortical attributes on sulci and gyri. To assess the underlying relationship between cortical thickness and fiber density, for the first time (as far as we know), we revealed that these two distinct cortical attributes had particularly strong positive correlations in several 3-hinge junction regions of gyri, where the fiber density has also been found significantly higher than that in 2-hinge gyri in adults (Li, et al. 2010). This result may suggest that the axonal wiring *not only* determines the cortical folding *but also* affects the cortical thickness in these junction regions of gyri, if this can be also replicated in other populations. Again, the “gyral bias” concept (Van Essen 2014) cannot well explain the significantly increased fiber densities on 3-hinge junction areas (Li, et al. 2010), since typically the surface curvatures in these 3-hinge areas are substantially smaller than those 2-hinge areas, where more biases should be observed according to the “gyral bias” concept. Instead, we believe that the mapping of DTI-derived fiber densities in those 3-hinge gyri reflects the true biological phenomenon. In addition, the negative correlation between tract density and cortical thickness in sulcal regions might suggest a different folding mechanism in sulci other than that in gyri. One possibility is that the stiff fiber tracts in the gyral regions constantly “push” the cortical plate such that the cortical layers have to grow in the tangential directions, thus gradually forming the sulci under the constraint of brain skull. Given the much less dense tract fibers connected in the sulci, more accumulation of neurons in the sulcal regions would result in a negative correlation between tract density and cortical thickness in these areas. We will extensively examine this hypothesis via both neuroimaging data analysis and computational simulation in our future work.

We should mention that, in this paper, we studied only the cross-subject correlation, i.e., the correlation between cortical thickness and fiber density across subjects at each vertex of each age group, as we are interested in the spatially-detailed correlation map between these two attributes. In fact, there also exist other two types of correlations: 1) within-subject temporal correlation (i.e., the correlation between cortical thickness and fiber density over all ages for each subject) and 2) within-subject spatial correlation (i.e., the correlation between cortical thickness map and fiber density map for each subject at each age). For example, as shown in Figure 3 and Figure 5, both cortical thickness and fiber density increase dynamically in the first year, suggesting positive within-subject temporal correlations. However, in the second year, the average cortical thickness in the sulcal regions decreases, while the corresponding fiber density still increases, thus indicating negative within-subject temporal correlations, although these two attributes both increase in the gyral regions. This further suggests differential growth mechanisms between sulci and gyri. In our future work, we will comprehensively study these three types of correlation in the large-scale longitudinal MRI datasets.

It should be caveated that one limitation of our current study is that streamline tractography from DTI has difficulty in accurately dealing with complex crossing fibers (Mori, et al. 1999). Nevertheless, previous studies in adults using advanced stochastic tractography and HARDI found similar distinct patterns of cortical fiber density between gyri and sulci, compared with the case of using streamline tractography, implying that these findings are independent of the tractography methods (Nie, et al. 2012a). Therefore, it is less likely that our findings on cortical fiber density between gyri and sulci in developing infants would change substantially when using stochastic tractography (Behrens, et al. 2003), which will be further verified in our future work. However, we should mention that tractography from diffusion MR imaging is an indirect method for studying axonal fibers at the macro-scale, which is affected by a set of factors, such as computational simulation methods and their parameter settings, and also the limited imaging resolutions. Hence, it is possible that some complicated axonal fibers, such as crossing fibers and U-shape fibers, cannot be revealed by the existing tractography studies. Also, the highly folded nature of the cortical surface might further cause false positives/negatives when fiber tracking approaches the cortex (Reveley, et al. 2015). Essentially, current diffusion imaging techniques are far from being able to accurately map the *complete* complex fiber pathways and connectional architectures of the cerebral cortex (Markov, et al. 2011; Schmahmann and Pandya 2006; Thomas, et al. 2014), although some studies in animals have demonstrated substantial similarities between diffusion imaging derived fiber pathways and invasive tracer injection results (Azadbakht, et al. 2015; Dauguet, et al. 2007; Dyrby, et al. 2007; Jbabdi, et al. 2013), which are frequently considered as the golden standard for the fiber pathways. With the availability of large-scale neuronal tracing data, such as the Allen Mouse Brain Connectivity Atlas (http://connectivity.brain-map.org), it becomes feasible to evaluate and validate DTI and DTI tractography methods based on the benchmark data of high-density axonal projections mapped by microscopic serial two-photon tomography (Chen, et al. 2015). In addition, DTI tractography methods and parameters could be potentially optimized in order to maximize both sensitivity and specificity of mapping real axons via the golden standard of neuronal tracing data, as shown in our recent study (Chen, et al. 2015).

In summary, for the first time (as far as we are aware), we systemically characterized the spatial distributions and longitudinal developmental trajectories of cortical fiber density in the first 2 postnatal years, via joint analysis of longitudinal structural and diffusion tensor MRI data from 33 healthy infants. We revealed several hitherto unseen patterns of cortical fiber density during the dynamic early postnatal stages, including 1) cortical fiber density increased dramatically in the first postnatal year and then changed relatively small in the second postnatal year; 2) cortical fiber density on gyri was significantly higher at 0, 1, and 2 years of age than that on sulci in the frontal, temporal, and parietal lobes; and 3) cortical fiber density was strongly positively correlated with cortical thickness at several junction regions of gyri. As all prior studies of cortical folding and axonal wiring in human brains have been largely focused on well-developed adults, our results on the developing infants significantly advance our understanding on the intrinsic relationship between cortical folding and axonal wiring in early postnatal stages, and also provide new evidence that largely supports the axonal pushing hypothesis of cortical folding (Chen, et al. 2013; Nie, et al. 2012a).

Acknowledgments

Funding

This work was supported in part by National Institutes of Health (MH100217, EB006733, EB008374, EB009634, MH088520, NS055754, HD053000, AG041721 and MH070890). G. Li was supported by NIH K01MH107815. T. Liu was supported by NIH DA033393, NIH AG042599, NSF IIS-1149260, NSF CBET-1302089 and NSF BCS-1439051.

References

Armstrong E, Schleicher A, Omran H, Curtis M, Zilles K. The ontogeny of human gyrification. Cereb Cortex. 1995; 5(1):56–63. [PubMed: 7719130]

Azadbakht H, Parkes LM, Haroon HA, Augath M, Logothetis NK, de Crespigny A, D'Arceuil HE, Parker GJ. Validation of High-Resolution Tractography Against In Vivo Tracing in the Macaque Visual Cortex. Cereb Cortex. 2015

Basser PJ, Mattiello J, Lebihan D. Estimation of the Effective Self-Diffusion Tensor from the Nmr Spin-Echo. Journal of Magnetic Resonance Series B. 1994; 103(3):247–254. [PubMed: 8019776]

Behrens TEJ, Johansen-Berg H, Woolrich MW, Smith SM, Wheeler-Kingshott CAM, Boulby PA, Barker GJ, Sillery EL, Sheehan K, Ciccarelli O, et al. Non-invasive mapping of connections between human thalamus and cortex using diffusion imaging. Nature Neuroscience. 2003; 6(7): 750–757. [PubMed: 12808459]

Carman GJ, Drury HA, Van Essen DC. Computational methods for reconstructing and unfolding the cerebral cortex. Cereb Cortex. 1995; 5(6):506–517. [PubMed: 8590824]

Chen H, Liu T, Zhao Y, Zhang T, Li Y, Li M, Zhang H, Kuang H, Guo L, Tsien JZ. Optimization of large-scale mouse brain connectome via joint evaluation of DTI and neuron tracing data. Neuroimage. 2015; 115:202–213. [PubMed: 25953631]

Chen H, Zhang T, Guo L, Li K, Yu X, Li L, Hu X, Han J, Liu T. Coevolution of gyral folding and structural connection patterns in primate brains. Cereb Cortex. 2013; 23(5):1208–1217. [PubMed: 22586139]

Chi JG, Dooling EC. Gyral development of the human brain. Trans Am Neurol Assoc. 1976; 101:89–90. [PubMed: 1036205]

Choe MS, Ortiz-Mantilla S, Makris N, Gregas M, Bacic J, Haehn D, Kennedy D, Pienaar R, Caviness VS Jr, Benasich AA, et al. Regional infant brain development: an MRI-based morphometric analysis in 3 to 13 month olds. Cereb Cortex. 2013; 23(9):2100–2117. [PubMed: 22772652]

Dauguet J, Peled S, Berezovskii V, Delzescaux T, Warfield SK, Born R, Westin CF. Comparison of fiber tracts derived from in-vivo DTI tractography with 3D histological neural tract tracer reconstruction on a macaque brain. Neuroimage. 2007; 37(2):530–538. [PubMed: 17604650]

Dubois J, Benders M, Cachia A, Lazeyras F, Ha-Vinh Leuchter R, Sizonenko SV, Borradori-Tolsa C, Mangin JF, Huppi PS. Mapping the early cortical folding process in the preterm newborn brain. Cereb Cortex. 2008a; 18(6):1444–1454. [PubMed: 17934189]

Dubois J, Dehaene-Lambertz G, Perrin M, Mangin JF, Cointepas Y, Duchesnay E, Le Bihan D, Hertz-Pannier L. Asynchrony of the early maturation of white matter bundles in healthy infants: quantitative landmarks revealed noninvasively by diffusion tensor imaging. Hum Brain Mapp. 2008b; 29(1):14–27. [PubMed: 17318834]

Dubois J, Hertz-Pannier L, Dehaene-Lambertz G, Cointepas Y, Le Bihan D. Assessment of the early organization and maturation of infants' cerebral white matter fiber bundles: a feasibility study using quantitative diffusion tensor imaging and tractography. Neuroimage. 2006; 30(4):1121–1132. [PubMed: 16413790]

Dyrby TB, Sogaard LV, Parker GJ, Alexander DC, Lind NM, Baare WF, Hay-Schmidt A, Eriksen N, Pakkenberg B, Paulson OB, et al. Validation of in vitro probabilistic tractography. Neuroimage. 2007; 37(4):1267–1277. [PubMed: 17706434]

Fischl B, Dale AM. Measuring the thickness of the human cerebral cortex from magnetic resonance images. Proc Natl Acad Sci U S A. 2000; 97(20):11050–11055. [PubMed: 10984517]

Fischl B, Sereno MI, Dale AM. Cortical surface-based analysis. II: Inflation, flattening, and a surface-based coordinate system. Neuroimage. 1999; 9(2):195–207. [PubMed: 9931269]

Gao W, Lin W, Chen Y, Gerig G, Smith JK, Jewells V, Gilmore JH. Temporal and spatial development of axonal maturation and myelination of white matter in the developing brain. AJNR Am J Neuroradiol. 2009a; 30(2):290–296. [PubMed: 19001533]

Gao W, Zhu H, Giovanello KS, Smith JK, Shen D, Gilmore JH, Lin W. Evidence on the emergence of the brain's default network from 2-week-old to 2-year-old healthy pediatric subjects. Proc Natl Acad Sci U S A. 2009b; 106(16):6790–6795. [PubMed: 19351894]

Geng X, Gouttard S, Sharma A, Gu H, Styner M, Lin W, Gerig G, Gilmore JH. Quantitative tract-based white matter development from birth to age 2years. Neuroimage. 2012; 61(3):542–557. [PubMed: 22510254]

Gilmore JH, Shi F, Woolson SL, Knickmeyer RC, Short SJ, Lin W, Zhu H, Hamer RM, Styner M, Shen D. Longitudinal development of cortical and subcortical gray matter from birth to 2 years. Cereb Cortex. 2012; 22(11):2478–2485. [PubMed: 22109543]

Grewen K, Burchinal M, Vachet C, Gouttard S, Gilmore JH, Lin W, Johns J, Elam M, Gerig G. Prenatal cocaine effects on brain structure in early infancy. Neuroimage. 2014; 101:114–123. [PubMed: 24999039]

Hazlett HC, Poe MD, Gerig G, Styner M, Chappell C, Smith RG, Vachet C, Piven J. Early Brain Overgrowth in Autism Associated With an Increase in Cortical Surface Area Before Age 2 Years. Archives of General Psychiatry. 2011; 68(5):467–476. [PubMed: 21536976]

He Y, Chen ZJ, Evans AC. Small-world anatomical networks in the human brain revealed by cortical thickness from MRI. Cereb Cortex. 2007; 17(10):2407–2419. [PubMed: 17204824]

Hill J, Dierker D, Neil J, Inder T, Knutsen A, Harwell J, Coalson T, Van Essen D. A surface-based analysis of hemispheric asymmetries and folding of cerebral cortex in term-born human infants. J Neurosci. 2010; 30(6):2268–2276. [PubMed: 20147553]

Holland D, Chang L, Ernst TM, Curran M, Buchthal SD, Alicata D, Skranes J, Johansen H, Hernandez A, Yamakawa R, et al. Structural growth trajectories and rates of change in the first 3 months of infant brain development. JAMA Neurol. 2014; 71(10):1266–1274. [PubMed: 25111045]

Jbabdi S, Lehman JF, Haber SN, Behrens TE. Human and Monkey Ventral Prefrontal Fibers Use the Same Organizational Principles to Reach Their Targets: Tracing versus Tractography. Journal of Neuroscience. 2013; 33(7):3190–3201. [PubMed: 23407972]

Knickmeyer RC, Gouttard S, Kang C, Evans D, Wilber K, Smith JK, Hamer RM, Lin W, Gerig G, Gilmore JH. A structural MRI study of human brain development from birth to 2 years. J Neurosci. 2008; 28(47):12176–12182. [PubMed: 19020011]

Kostovic I, Jovanov-Milosevic N. The development of cerebral connections during the first 20–45 weeks' gestation. Semin Fetal Neonatal Med. 2006; 11(6):415–422. [PubMed: 16962836]

Li G, Guo L, Nie J, Liu T. Automatic cortical sulcal parcellation based on surface principal direction flow field tracking. Neuroimage. 2009; 46(4):923–937. [PubMed: 19328234]

Li G, Lin W, Gilmore JH, Shen D. Spatial Patterns, Longitudinal Development, and Hemispheric Asymmetries of Cortical Thickness in Infants from Birth to 2 Years of Age. J Neurosci. 2015a; 35(24):9150–9162. [PubMed: 26085637]

Li G, Nie J, Wang L, Shi F, Gilmore JH, Lin W, Shen D. Measuring the dynamic longitudinal cortex development in infants by reconstruction of temporally consistent cortical surfaces. Neuroimage. 2014a; 90:266–279. [PubMed: 24374075]

Li G, Nie J, Wang L, Shi F, Lin W, Gilmore JH, Shen D. Mapping region-specific longitudinal cortical surface expansion from birth to 2 years of age. Cereb Cortex. 2013; 23(11):2724–2733. [PubMed: 22923087]

Li G, Nie J, Wang L, Shi F, Lyall AE, Lin W, Gilmore JH, Shen D. Mapping longitudinal hemispheric structural asymmetries of the human cerebral cortex from birth to 2 years of age. Cereb Cortex. 2014b; 24(5):1289–1300. [PubMed: 23307634]

Li G, Nie J, Wu G, Wang Y, Shen D. Consistent reconstruction of cortical surfaces from longitudinal brain MR images. Neuroimage. 2012; 59(4):3805–3820. [PubMed: 22119005]

Li G, Wang L, Shi F, Gilmore JH, Lin W, Shen D. Construction of 4D high-definition cortical surface atlases of infants: Methods and applications. Med Image Anal. 2015b

Li G, Wang L, Shi F, Lyall AE, Ahn M, Peng Z, Zhu H, Lin W, Gilmore JH, Shen D. Cortical thickness and surface area in neonates at high risk for schizophrenia. Brain Structure and Function. 2014c:1–15. [PubMed: 23474540]

Li G, Wang L, Shi F, Lyall AE, Lin W, Gilmore JH, Shen D. Mapping longitudinal development of local cortical gyrification in infants from birth to 2 years of age. J Neurosci. 2014d; 34(12):4228–4238. [PubMed: 24647943]

Li K, Guo L, Li G, Nie J, Faraco C, Cui G, Zhao Q, Miller LS, Liu T. Gyral folding pattern analysis via surface profiling. Neuroimage. 2010; 52(4):1202–1214. [PubMed: 20472071]

Lyall AE, Shi F, Geng X, Woolson S, Li G, Wang L, Hamer RM, Shen D, Gilmore JH. Dynamic Development of Regional Cortical Thickness and Surface Area in Early Childhood. Cereb Cortex. 2015; 25(8):2204–2212. [PubMed: 24591525]

Markov NT, Misery P, Falchier A, Lamy C, Vezoli J, Quilodran R, Gariel MA, Giroud P, Ercsey-Ravasz M, Pilaz LJ, et al. Weight consistency specifies regularities of macaque cortical networks. Cereb Cortex. 2011; 21(6):1254–1272. [PubMed: 21045004]

Meng Y, Li G, Lin W, Gilmore JH, Shen D. Spatial distribution and longitudinal development of deep cortical sulcal landmarks in infants. Neuroimage. 2014; 100C:206–218. [PubMed: 24945660]

Mori S, Crain BJ, Chacko VP, van Zijl PC. Three-dimensional tracking of axonal projections in the brain by magnetic resonance imaging. Ann Neurol. 1999; 45(2):265–269. [PubMed: 9989633]

Nie J, Guo L, Li K, Wang Y, Chen G, Li L, Chen H, Deng F, Jiang X, Zhang T, et al. Axonal fiber terminations concentrate on gyri. Cereb Cortex. 2012a; 22(12):2831–2839. [PubMed: 22190432]

Nie J, Li G, Shen D. Development of cortical anatomical properties from early childhood to early adulthood. Neuroimage. 2013; 76:216–224. [PubMed: 23523806]

Nie J, Li G, Wang L, Gilmore JH, Lin W, Shen D. A computational growth model for measuring dynamic cortical development in the first year of life. Cereb Cortex. 2012b; 22(10):2272–2284. [PubMed: 22047969]

Nie J, Li G, Wang L, Shi F, Lin W, Gilmore JH, Shen D. Longitudinal development of cortical thickness, folding, and fiber density networks in the first 2 years of life. Hum Brain Mapp. 2014; 35(8):3726–3737. [PubMed: 24375724]

Ono, M.; Kubik, S.; Abernathey, CD. Atlas of the cerebral sulci. Stuttgart: G. Thieme Verlag ; New York: Thieme Medical Publishers; 1990. p. 218xiv

Qiu A, Mori S, Miller MI. Diffusion tensor imaging for understanding brain development in early life. Annu Rev Psychol. 2015; 66:853–876. [PubMed: 25559117]

Reveley C, Seth AK, Pierpaoli C, Silva AC, Yu D, Saunders RC, Leopold DA, Ye FQ. Superficial white matter fiber systems impede detection of long-range cortical connections in diffusion MR tractography. Proceedings of the National Academy of Sciences of the United States of America. 2015; 112(21):E2820–E2828. [PubMed: 25964365]

Rimol LM, Hartberg CB, Nesvag R, Fennema-Notestine C, Hagler DJ Jr, Pung CJ, Jennings RG, Haukvik UK, Lange E, Nakstad PH, et al. Cortical thickness and subcortical volumes in schizophrenia and bipolar disorder. Biol Psychiatry. 2010; 68(1):41–50. [PubMed: 20609836]

Sadeghi N, Prastawa M, Fletcher PT, Wolff J, Gilmore JH, Gerig G. Regional characterization of longitudinal DT-MRI to study white matter maturation of the early developing brain. Neuroimage. 2013; 68:236–247. [PubMed: 23235270]

Schmahmann, JD.; Pandya, DN. Fiber pathways of the brain. Oxford ; New York: Oxford University Press; 2006. p. 654xviii

Shaw P, Kabani NJ, Lerch JP, Eckstrand K, Lenroot R, Gogtay N, Greenstein D, Clasen L, Evans A, Rapoport JL, et al. Neurodevelopmental trajectories of the human cerebral cortex. J Neurosci. 2008; 28(14):3586–3594. [PubMed: 18385317]

Shaw P, Lerch J, Greenstein D, Sharp W, Clasen L, Evans A, Giedd J, Castellanos FX, Rapoport J. Longitudinal mapping of cortical thickness and clinical outcome in children and adolescents with attention-deficit/hyperactivity disorder. Arch Gen Psychiatry. 2006; 63(5):540–549. [PubMed: 16651511]

Shen D, Davatzikos C. HAMMER: hierarchical attribute matching mechanism for elastic registration. IEEE Trans Med Imaging. 2002; 21(11):1421–1439. [PubMed: 12575879]

Shi F, Wang L, Dai Y, Gilmore JH, Lin W, Shen D. LABEL: Pediatric brain extraction using learning-based meta-algorithm. Neuroimage. 2012; 62(3):1975–1986. [PubMed: 22634859]

Shi F, Yap PT, Wu G, Jia H, Gilmore JH, Lin W, Shen D. Infant brain atlases from neonates to 1- and 2-year-olds. PLoS One. 2011; 6(4):e18746. [PubMed: 21533194]

Sled JG, Zijdenbos AP, Evans AC. A nonparametric method for automatic correction of intensity nonuniformity in MRI data. IEEE Trans Med Imaging. 1998; 17(1):87–97. [PubMed: 9617910]

Sowell ER, Thompson PM, Leonard CM, Welcome SE, Kan E, Toga AW. Longitudinal mapping of cortical thickness and brain growth in normal children. J Neurosci. 2004; 24(38):8223–8231. [PubMed: 15385605]

Takahashi E, Folkerth RD, Galaburda AM, Grant PE. Emerging cerebral connectivity in the human fetal brain: an MR tractography study. Cereb Cortex. 2012; 22(2):455–464. [PubMed: 21670100]

Thomas C, Ye FQ, Irfanoglu MO, Modi P, Saleem KS, Leopold DA, Pierpaoli C. Anatomical accuracy of brain connections derived from diffusion MRI tractography is inherently limited. Proceedings of the National Academy of Sciences of the United States of America. 2014; 111(46): 16574–16579. [PubMed: 25368179]

Van Essen DC. A tension-based theory of morphogenesis and compact wiring in the central nervous system. Nature. 1997; 385(6614):313–318. [PubMed: 9002514]

Van Essen DC. Cartography and connectomes. Neuron. 2013; 80(3):775–790. [PubMed: 24183027]

Van Essen DC, Drury HA. Structural and functional analyses of human cerebral cortex using a surface-based atlas. J Neurosci. 1997; 17(18):7079–7102. [PubMed: 9278543]

Van Essen, DC.; Jbabdi, S.; Sotiropoulos, SN.; Chen, C.; Dikranian, K.; Coalson, T.; Harwell, J.; Behrens, TEJ.; Glasser, MF. Mapping connections in humans and nonhuman primates: Aspirations and challenges for diffusion imaging. In: Johansen-Berg, H.; Behrens, TEJ., editors. Diffusion MRI : from quantitative measurement to in-vivo neuroanatomy. 2nd ed.. London, UK ; Waltham, MA: Elsevier/Academic Press; 2014.

Wang L, Shi F, Li G, Gao Y, Lin W, Gilmore JH, Shen D. Segmentation of neonatal brain MR images using patch-driven level sets. Neuroimage. 2013a; 84C:141–158. [PubMed: 23968736]

Wang L, Shi F, Yap PT, Lin W, Gilmore JH, Shen D. Longitudinally guided level sets for consistent tissue segmentation of neonates. Hum Brain Mapp. 2013b; 34(4):956–972. [PubMed: 22140029]

Wolff JJ, Gerig G, Lewis JD, Soda T, Styner MA, Vachet C, Botteron KN, Elison JT, Dager SR, Estes AM, et al. Altered corpus callosum morphology associated with autism over the first 2 years of life. Brain. 2015; 138(Pt 7):2046–2058. [PubMed: 25937563]

Wolff JJ, Gu H, Gerig G, Elison JT, Styner M, Gouttard S, Botteron KN, Dager SR, Dawson G, Estes AM, et al. Differences in white matter fiber tract development present from 6 to 24 months in infants with autism. Am J Psychiatry. 2012; 169(6):589–600. [PubMed: 22362397]

Yap PT, Fan Y, Chen Y, Gilmore JH, Lin W, Shen D. Development trends of white matter connectivity in the first years of life. PLoS One. 2011; 6(9):e24678. [PubMed: 21966364]

Yeo BT, Sabuncu MR, Vercauteren T, Ayache N, Fischl B, Golland P. Spherical demons: fast diffeomorphic landmark-free surface registration. IEEE Trans Med Imaging. 2010; 29(3):650–668. [PubMed: 19709963]

Zeng T, Chen H, Fakhry A, Hu X, Liu T, Ji S. Allen mouse brain atlases reveal different neural connection and gene expression patterns in cerebellum gyri and sulci. Brain Struct Funct. 2014

Zhang, DG.; Guo, L.; Li, G.; Nie, JX.; Deng, F.; Li, KM.; Hu, XT.; Zhang, T.; Jiang, X.; Zhu, DJ., et al. Automatic Cortical Surface Parcellation Based on Fiber Density Information; 2010 7th Ieee International Symposium on Biomedical Imaging: From Nano to Macro; 2010. p. 1133-1136.

Zhang T, Chen H, Guo L, Li K, Li L, Zhang S, Shen D, Hu X, Liu T. Characterization of U-shape streamline fibers: Methods and applications. Med Image Anal. 2014; 18(5):795–807. [PubMed: 24835185]

Zhu HT, Zhang HP, Ibrahim JG, Peterson BS. Statistical analysis of diffusion tensors in diffusion-weighted magnetic resonance imaging data. Journal of the American Statistical Association. 2007; 102(480):1085–1102.

Zilles K, Armstrong E, Moser KH, Schleicher A, Stephan H. Gyrification in the cerebral cortex of primates. Brain Behav Evol. 1989; 34(3):143–150. [PubMed: 2512000]

Zilles K, Palomero-Gallagher N, Amunts K. Development of cortical folding during evolution and ontogeny. Trends Neurosci. 2013; 36(5):275–284. [PubMed: 23415112]

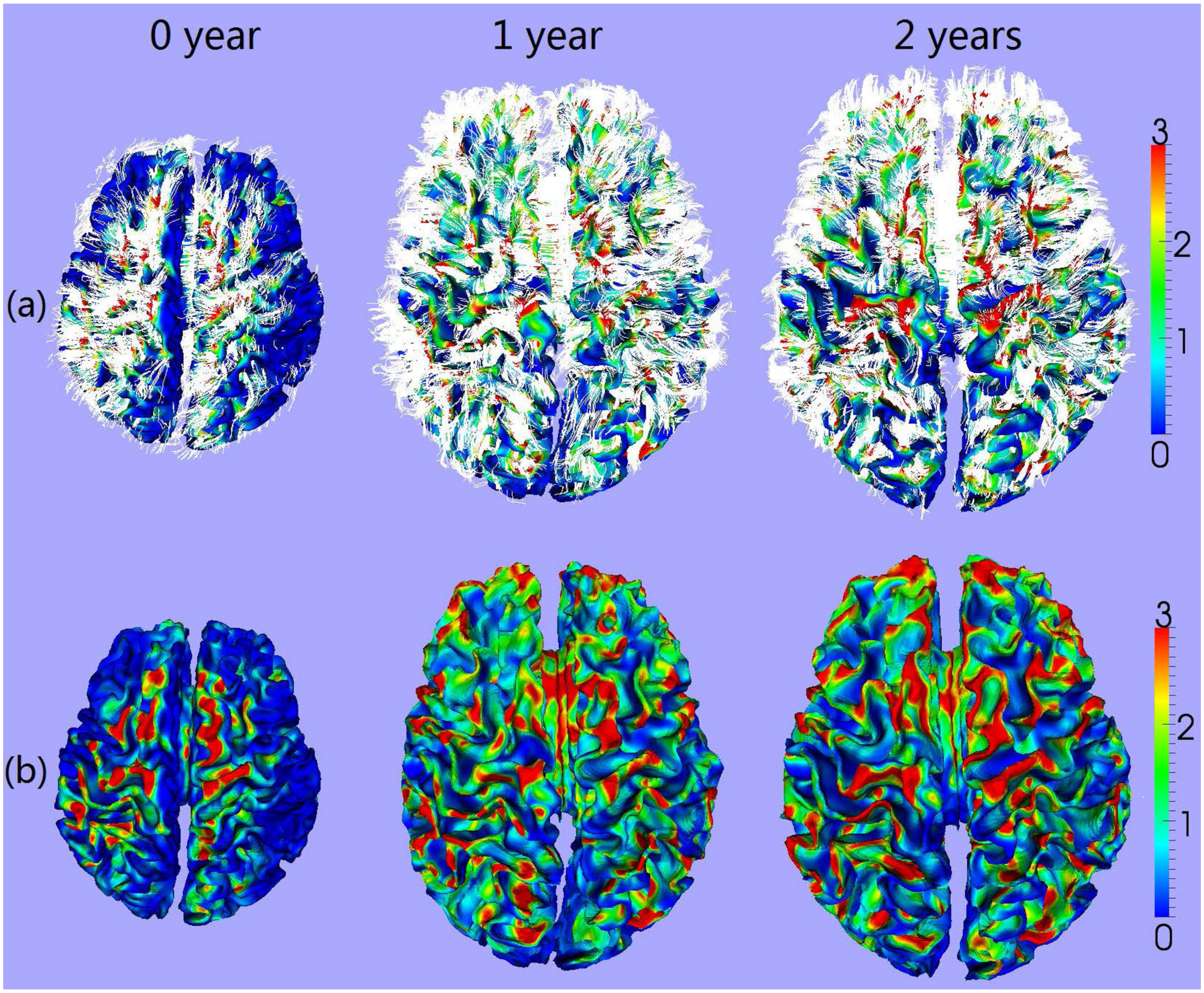

Figure 1.

Cortical fiber density on a representative developing infant at 0, 1, and 2 years of age. (a) Overlaying the fibers (white streamlines) with the cortical surfaces. (b) Fiber density on the cortical surfaces. The color bars are shown on the right.

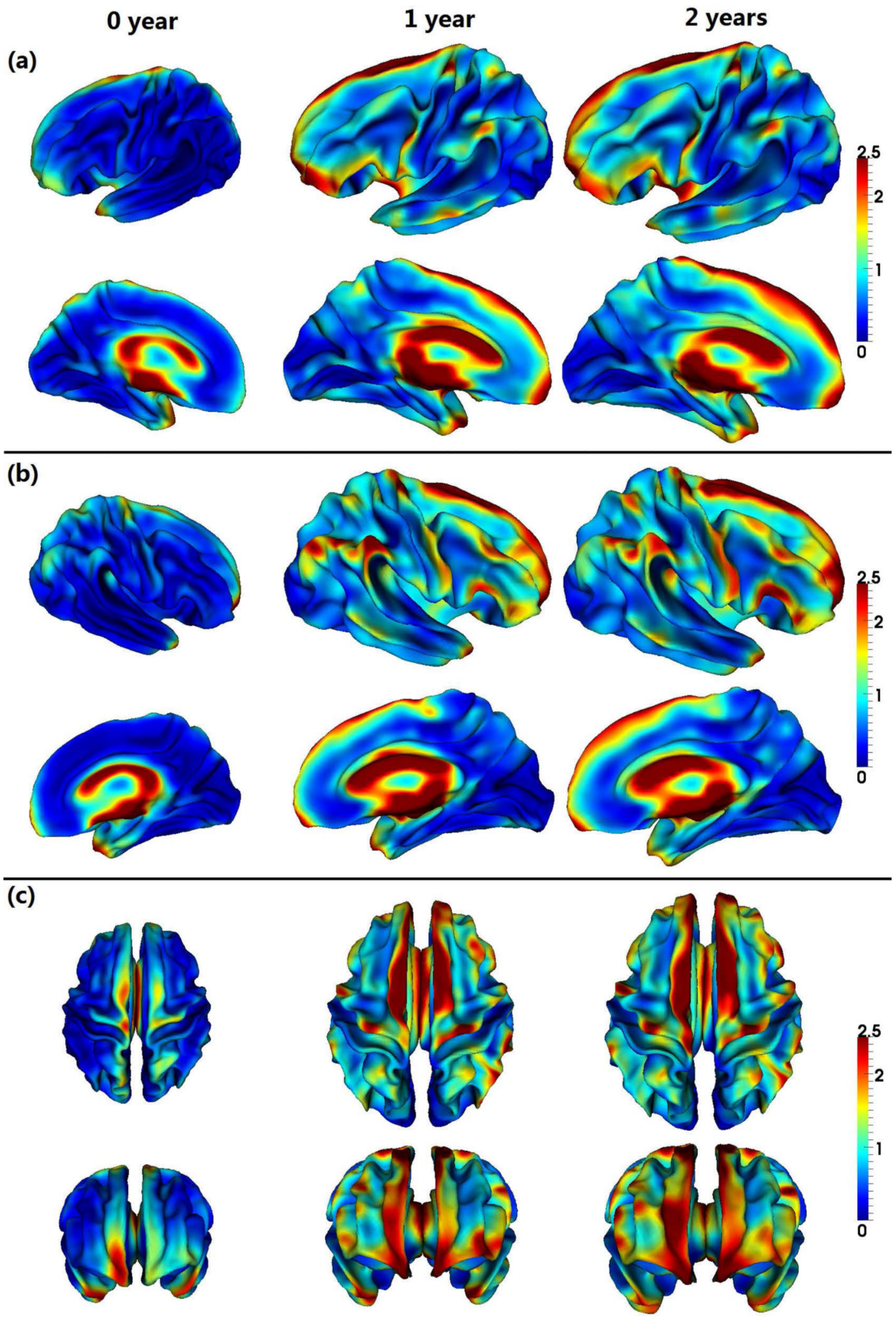

Figure 2.

Spatial distributions of the average fiber density (/mm^2) on cortical surfaces from 33 infants, at 0, 1, and 2 years of age. Warm colors indicate high fiber density, and cold colors indicate low fiber density.

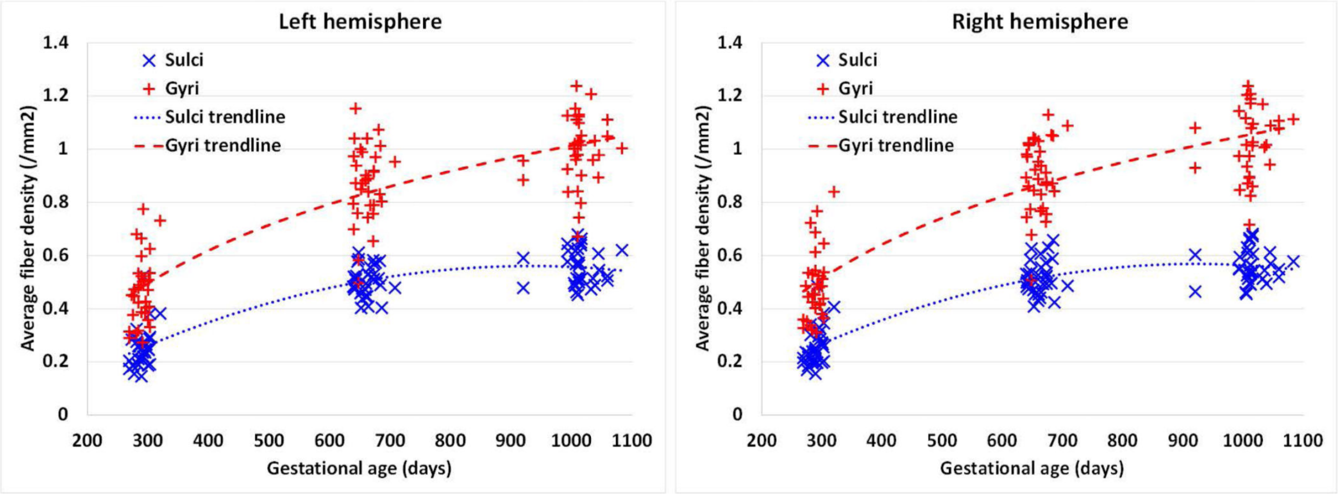

Figure 3.

Scatter plots of the average cortical fiber density in the sulcal and gyral regions, respectively, across the whole cortex of 33 infants at 0, 1, and 2 years of age.

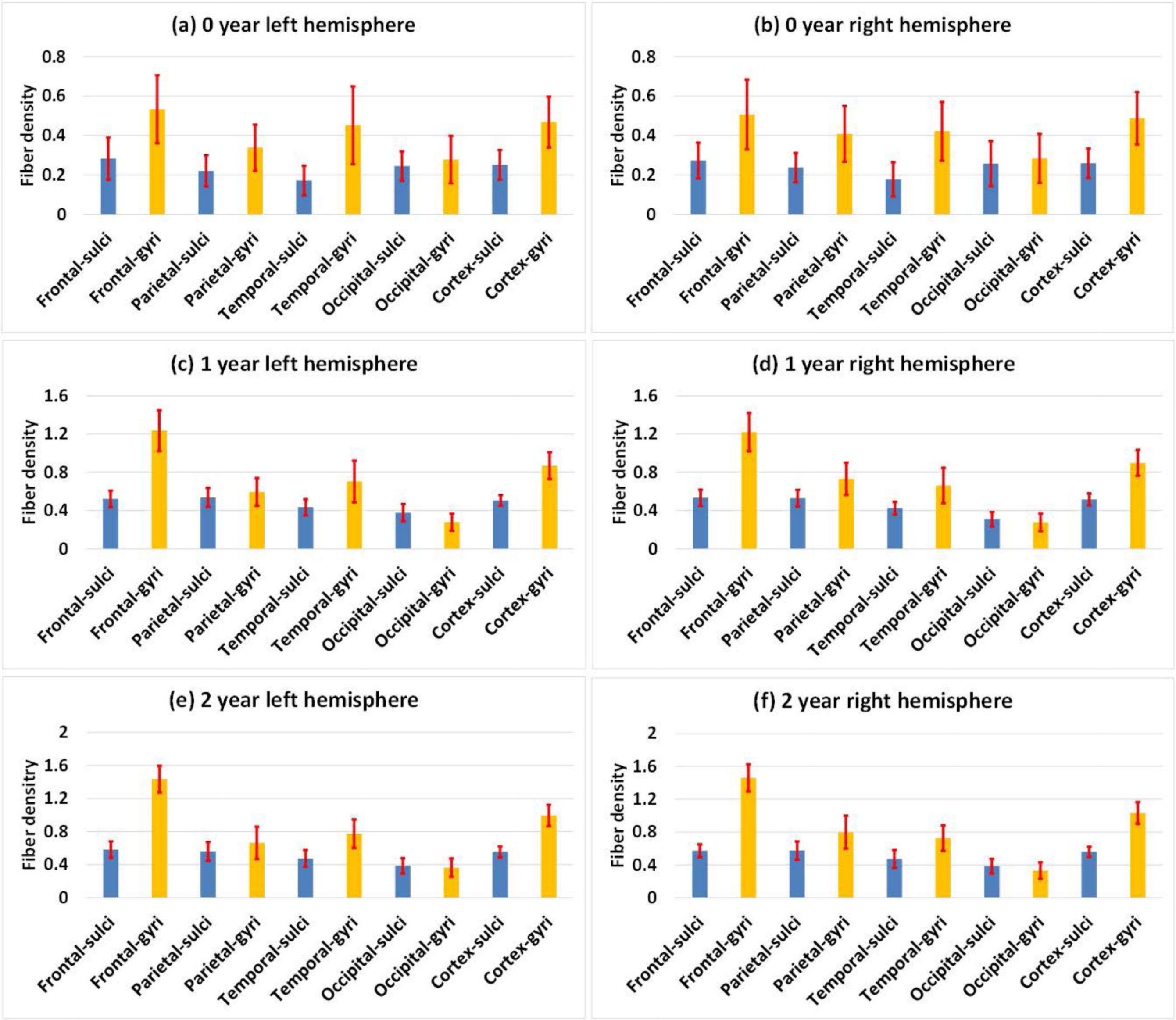

Figure 4.

Means and standard deviations of the cortical fiber density (/mm^2) in the sulcal and gyral regions of four lobes and the whole cortex from 33 infants at 0, 1, and 2 years of age.

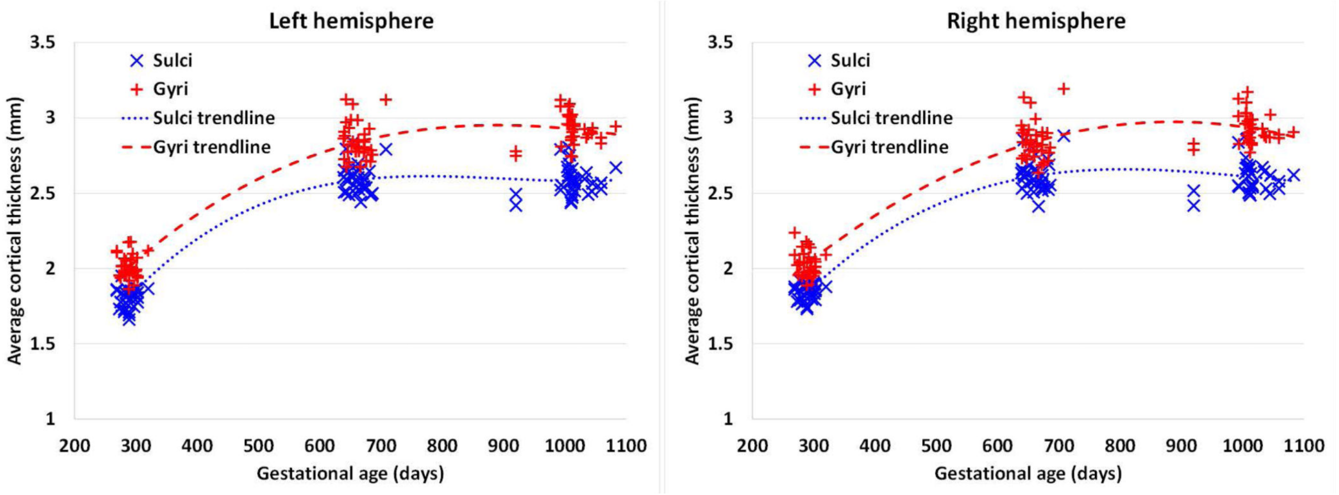

Figure 5.

Scatter plots of the average cortical thickness in the sulcal and gyral regions, respectively, across the whole cortex of 33 infants at 0, 1, and 2 years of age.

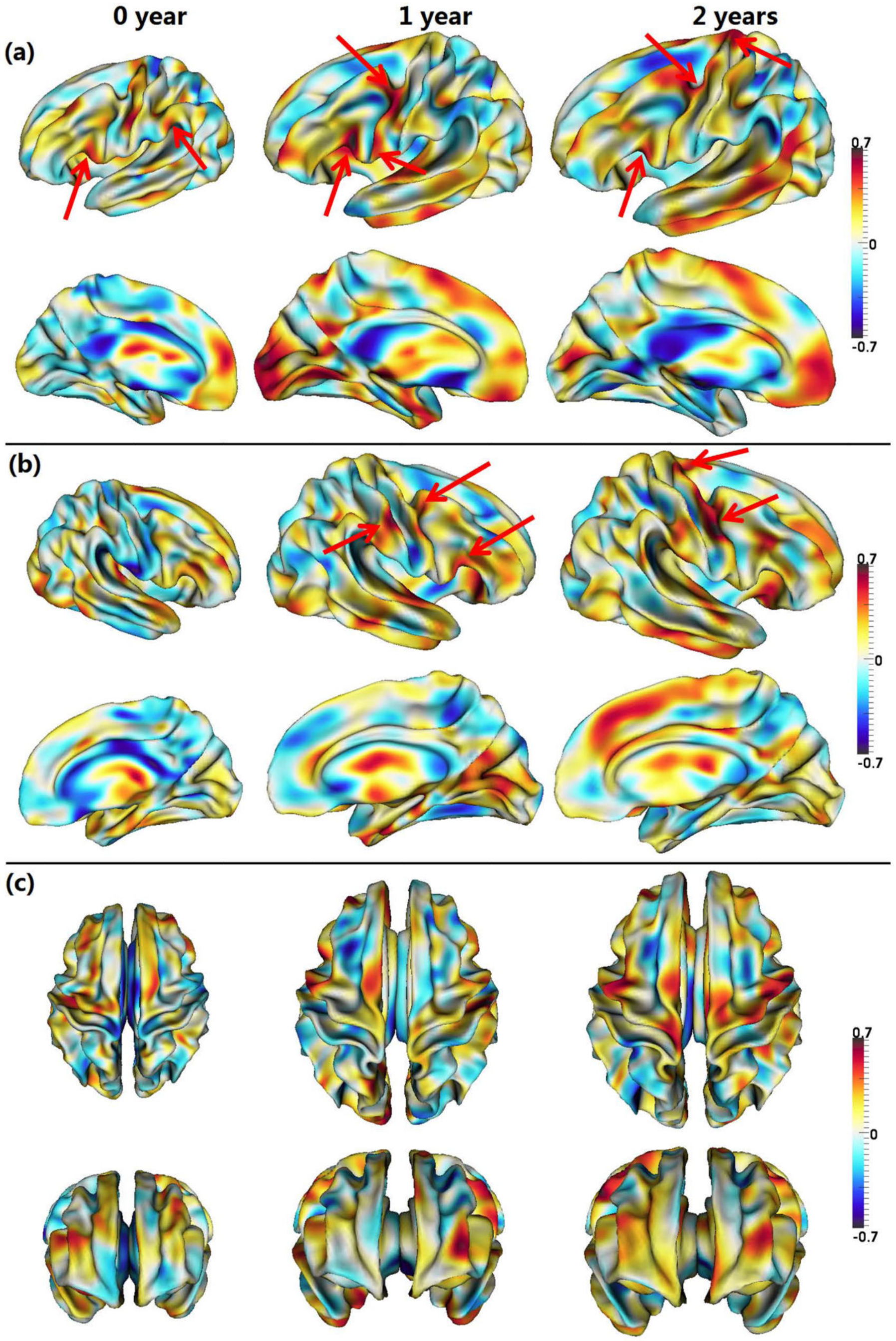

Figure 6.

Pearson’s correlation coefficients between the cortical fiber density and cortical thickness from 33 infants at 0, 1, and 2 years of age. Warm colors indicate strong positive correlation, while cool colors indicate strong negative correlation. Red arrows point out several regions with strong positive correlations. Pictures in (a–c) show correlation maps in different views.

Table 1

Ratios of the cortical fiber density on gyri *vs* those on sulci at 0, 1, and 2 years of age. Left: left hemisphere; Right: right hemisphere.

	0 year		**1 year**		**2 years**	
Regions	**Left**	**Right**	**Left**	**Right**	**Left**	**Right**
Frontal lobe	2.00±0.69	1.92±0.53	2.46±0.66	2.36±0.58	2.54±0.55	2.61±0.56
Parietal lobe	1.61±0.48	1.78±0.55	1.17±0.41	1.43±0.44	1.28±0.58	1.48±0.56
Temporal lobe	2.87±1.25	2.70±1.17	1.68±0.56	1.61±0.56	1.68±0.48	1.61±0.51
Occipital lobe	1.19±0.54	1.22±0.69	0.74±0.20	0.90±0.25	0.95±0.26	0.87±0.23
Whole cortex	1.91±0.44	1.93±0.40	1.75±0.38	1.77±0.36	1.83±0.39	1.88±0.38

Table 2

Statistical significance of the cortical fiber density difference between sulci and gyri at 0, 1, and 2 years of age. Bold values indicate p-values smaller than 0.05. Left: left hemisphere; Right: right hemisphere.

p-values	**0 year**		**1 year**		**2 years**	
Regions	**Left**	**Right**	**Left**	**Right**	**Left**	**Right**
Frontal lobe	**1.00E-11**	**2.87E-11**	**4.41E-16**	**5.00E-17**	**4.57E-21**	**1.86E-21**
Parietal lobe	**1.04E-07**	**3.79E-09**	**0.0236**	**2.36E-06**	**0.0179**	**4.93E-05**
Temporal lobe	**5.46E-10**	**5.26E-12**	**1.01E-07**	**1.20E-07**	**1.76E-10**	**2.68E-08**
Occipital lobe	0.133	0.206	**9.14E-08**	**0.0295**	0.1972	**0.0029**
Whole cortex	**2.93E-14**	**1.53E-14**	**1.97E-13**	**5.10E-15**	**1.46E-15**	**2.17E-16**